Reconfigurable All-Pass-to-Bandstop Acoustic-Wave-Lumped-Element Resonator Filters

Dimitra Psychogiou, *Senior Member, IEEE*

***Abstract*—Acoustic-wave lumped-element resonator (AWLR)-based filters with reconfigurable all-pass-to-bandstop transfer function are reported. They are based on in-series cascaded resonant stages that comprise two parallel RF signal paths, namely: 1) a thru-line and 2) an AWLR-based resonant section. Reconfigurability is achieved by altering the phase of the thru-line through varactors. In this manner, the filter response can be reconfigured from an all-pass to an enhanced fractional bandwidth (FBW)—i.e., wider than the electromechanical coupling coefficient k_t^2—bandstop one. For practical validation, two prototypes were designed and tested. They include 1) a single-stage prototype with insertion loss (IL) < 0.38 dB in the all-pass mode and a bandstop mode with a center frequency of 917.5 MHz, an FBW of 0.29% (2.4 k_t^2), and a stopband isolation of 21.2 dB and 2) a two-stage prototype that exhibits an all-pass mode with IL < 0.67 dB and a bandstop mode centered at 916.9 MHz, with an FBW of 0.47% (3.8 k_t^2) and a tunable isolation between 20 and 43 dB.**

***Index Terms*—Acoustic-wave filter, bandstop filter, kt2 enhancement, microwave filter, reconfigurable filter.**

I. Introduction

EMERGING 5G transceivers will be required to support a large number of applications with diverse requirements in terms of frequency and bandwidth. In addition, they will need to suppress interference when closely-spaced carriers share unlicensed bands [1]. To facilitate this functionality, filters with the ability to receive or reject an incoming RF signal will need to be incorporated in their receivers. However, most of the existing acoustic-wave resonator (AWR) filters using surface-acoustic-wave (SAW) or bulk-acoustic-wave (BAW) resonators [2] are frequency static and cannot realize bandstop-type responses. Furthermore, they (e.g., [2]–[7]) are limited by narrow fractional bandwidths (FBWs) that are smaller than the electromechanical coupling coefficient (k_t^2).

Recent research efforts on transfer function reconfigurability are mostly focused on switched SAW/BAW filter banks [4], [5] or intrinsically switched thin-film bulk acoustic resonator bandpass filters [6], [7]. In these filters, the bandpass-to-all-stop response is obtained by biasing their ferroelectric substrate [6], [7]. Intrinsically switchable AlGaN/GaN resonators were also shown in [8]. However, they exhibit high insertion loss (IL) of about 60 dB. In yet another configuration, AWRs are effectively combined with electromagnetic (EM) resonators—the so-called acoustic-wave-lumped-element resonator (AWLR) concept—to functionalize a wide variety of single- or multiband transfer functions (e.g., bandpass [9] and bandstop [10]) with enhanced FBW—i.e.,> k_t^2. Reconfigurability in FBW, transfer function, and out-of-band rejection [9]–[11] were also obtained.

Manuscript received May 22, 2020; accepted June 14, 2020. Date of publication July 10, 2020; date of current version August 7, 2020. This work was supported in part by the National Science Foundation under Grant ECCS-1731956.

The author is with the Department of Electrical, Computer, and Energy Engineering, University of Colorado Boulder, Boulder, CO 80309 USA (e-mail: dimitra.psychogiou@colorado.edu).

Color versions of one or more of the figures in this letter are available online at http://ieeexplore.ieee.org.

Digital Object Identifier 10.1109/LMWC.2020.3004028

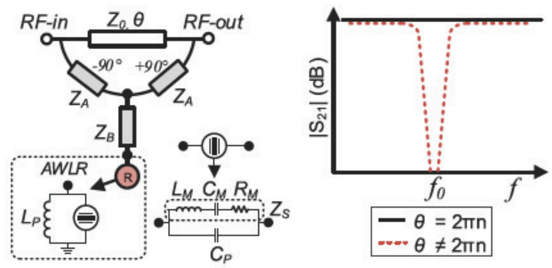

Fig. 1. Block diagram and conceptual power transmission response of the all-pass-to-bandstop AWLR stage. It consists of two parallel cascaded signal paths shaped by: 1) a transmission line with characteristic impedance Z_0 and electrical length θ at f_0 and by 2) a resonant signal path shaped by three inverters Z_A, Z_B and one AWLR (parallel combination of an AWR and an inductor L_P).

This letter explores for the first time, new types of electronically reconfigurable AWLR-based filters for RF receivers with the ability to acquire a wideband of the spectrum or to reject an interference-dominated channel. The proposed filter concept is based on in-series cascaded all-pass-to-bandstop AWLR stages—shaped by a tunable-phase thru-line and a resonant bandpass section—that facilitate: 1) a low-IL all-pass mode of operation and 2) a bandstop mode with enhanced FBW stopbands—i.e., > k_t^2—and tunable rejection levels.

II. Theoretical Foundations

The AWLR all-pass-to-bandstop filter concept is based on in-series cascaded all-pass-to-bandstop-reconfigurable stages that comprise two parallel RF signal paths shaped by: 1) a transmission line with characteristic impedance Z_0 and electrical length θ and 2) a bandpass-type resonant section that consists of three impedance inverters (Z_A, Z_B) and one AWLR as shown in Fig. 1. The AWLR is a high-quality-factor (Q) resonator shaped by the parallel combination of an AWR (C_M: motional capacitance, L_M: motional inductance, R_M: motional resistance, C_P: parallel capacitance as defined in its Butterworth–Van-Dyke (BVD) model) and an inductor L_P that resonates with C_P at the design frequency f_0 which is approximately equal to the series resonance f_S of the AWR. Further details on the AWLR principles are reported in [9].

By appropriately selecting the circuit parameters of the all-pass-to-bandstop stage, two modes of operation can be supported within the same device and tuned by altering θ (defined at f_0) as shown in Fig. 1. Z_As are set to have the same impedance and opposite phase. Thus, the all-pass mode is obtained when $\theta = 2\pi n, n \in Z$, whereas the bandstop mode when either of (1) or (2) is satisfied (obtained by setting $|S_{21}| = 0$). Z_S is the impedance of the AWLR at the

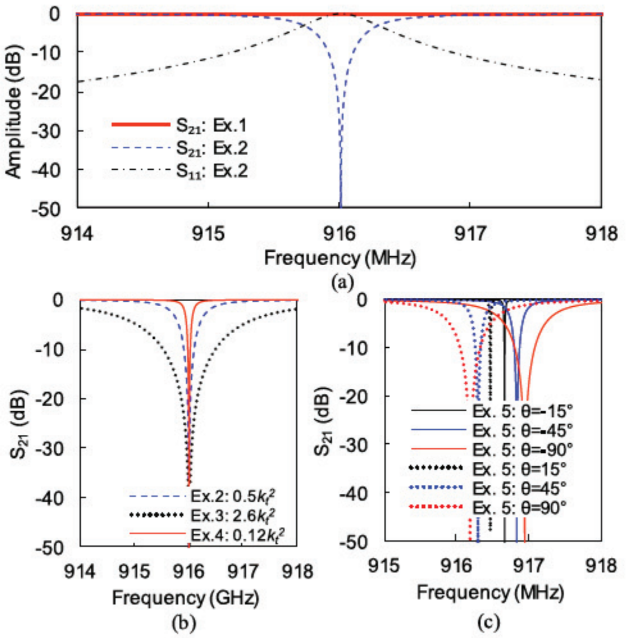

Fig. 2. Theoretical power transmission and reflection response of the reconfigurable all-pass-to-bandstop AWLR stage. (a) Example case of a single stage when θ is altered between 0° and 54°. (b) Design examples showing alternative FBWs and the filter's capability to realize bandstop modes of operation with FBWs > k_t^2. (c) Effect of θ tuning.

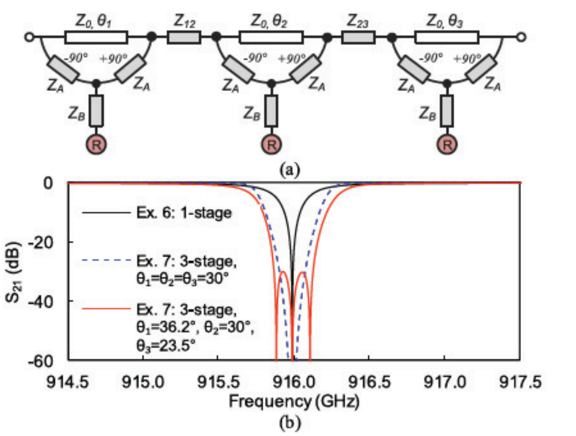

Fig. 3. Circuit schematic and theoretical power transmission response of a three-stage all-pass-to-bandstop AWLR-based filter. (a) Circuit schematic—stages cascaded with inverters (Z_{12}, Z_{23}). (b) Theoretical power transmission response for equal and unequal thru-line phases which result in single-notch and equiripple stopbands. A comparison with a single stage is also shown.

design frequency approximately equal to the impedance of the motional branch of the AWR

$$Z_S = 0, \quad \theta = 2\pi n + \pi, \ n \in Z \tag{1}$$

$$Z_S Z_A^2 = -i \sin\theta Z_0 Z_B^2, \quad \theta \neq 2\pi n, \ n \in Z. \tag{2}$$

To demonstrate the operating principles of the AWLR-based all-pass-to-bandstop filter concept, various examples are considered for a frequency around 916 MHz and an AWLR that is shaped by a commercially available AWR from Murata RO3144 ($C_M = 1.8475$ fF, $L_M = 16.32$ μH, $R_M = 17$ Ω, $C_P = 2.16$ pF, $f_S = 916.5$ MHz—extracted by fitting its measured S-parameters to the BVD model [9]) and are shown in Figs. 2 and 3. The element values for these examples are provided in Table I. In particular, Fig. 2(a) shows that the transfer function of the stage can be reconfigured between the all-pass mode and the bandstop mode by altering θ

TABLE I

COMPONENT VALUES FOR THE DESIGN EXAMPLES IN FIGS. 2 AND 3

Example	1	2	3	4	5	6	7
θ	0°	54°	138°	14.2°	VAR	30°	VAR
Z_A	80 Ω	80 Ω	80 Ω	80 Ω	80 Ω	80 Ω	80 Ω
Z_B	135 Ω	135 Ω	148 Ω	245 Ω	100 Ω	175 Ω	175 Ω

*VAR: Variable parameter, in these examples θ defined at f_S

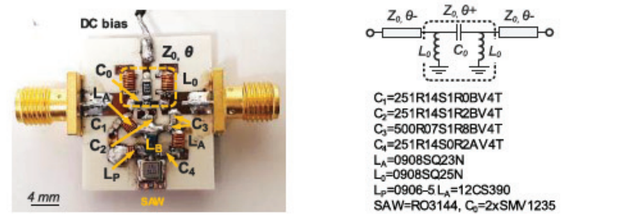

Fig. 4. Manufactured prototype and details of the tunable thru-line of the single-stage prototype. The SMD components are listed at the right side of the figure.

from 0° to 54° which can be readily implemented by using a tunable capacitor within an artificial transmission line as it will be explained in Section III. Furthermore, as shown in Fig. 2(b), when operating in the bandstop mode, the stage can be designed for FBWs—function of θ, Z_A, and Z_B—that are narrower or wider than the k_t^2 of the AWR allowing for enhanced FBW stopbands (FBW > k_t^2). Note that conventional AWR filters (in [2]–[7]) are limited by FBWs between 0.4 and 0.8 k_t^2. Lastly, Fig. 2(c) shows how the bandstop response changes when only θ is altered.

The selectivity and stopband profile of the bandstop mode can be altered by cascading multiple all-pass-to-bandstop stages through inverters. This is shown in Fig. 3(a) for the case of a three-stage filter. Its theoretical power transmission response in the bandstop mode is plotted in Fig. 3(b) alongside the one of a single stage to demonstrate the selectivity enhancement of the cascade approach. Although not shown in this figure, the all-pass response is obtained by setting $\theta_1 = \theta_2 = \theta_3 = 0°$ or 360°. Furthermore, Fig. 3(b) shows how alternative stopband profiles can be created by altering the phase of the thru-line in each stage which may result in single-notch ($\theta_1 = \theta_2 = \theta_3$) or equiripple stopbands ($\theta_1 \neq \theta_2 \neq \theta_3$). Similarly, higher order transfer functions can be obtained by cascading additional stages.

III. EXPERIMENTAL VALIDATION

For proof-of-concept validation purposes, a single-stage and a two-stage all-pass-to-bandstop prototypes were designed, manufactured, and measured. A hybrid integration scheme using commercially available SAW resonators (Murata RO3144), surface mount devices (SMDs), and a Rogers 4003 substrate was employed. The design of the filters was performed with the EM simulations in ADS Keysight using as a basis the design guidelines in Section II. In particular, the thru-line was made from two short microstrip transmission lines (Z_0, $\theta-$) and a tunable-phase artificial transmission line (Z_0, $\theta+$), implemented by its π-type high-pass equivalent. As shown in Fig. 4, two back-to-back varactors (SMV1235) were employed to vary its phase shift. The overall thru-line was designed for a variable phase between 0° (bias: 0 V) and 33° (bias: 10 V) at 916.5 MHz.

The single-stage prototype and its components are shown in Fig. 4 for a design frequency of 917.5 MHz. The measured reconfigurable bandstop and all-pass modes are plotted in Fig. 5(a) and (b). It exhibits 1) an all-pass mode with IL

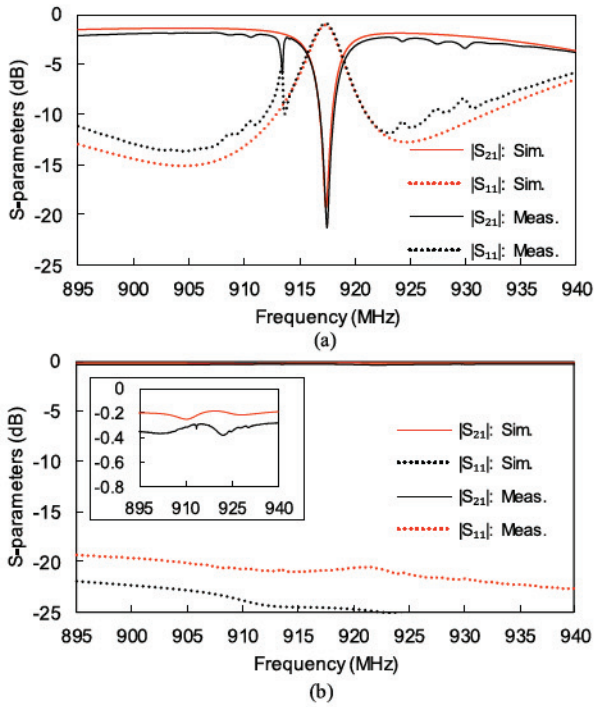

Fig. 5. RF-measured and EM-simulated S-parameters of the single-stage all-pass-to-bulk shielding facility (BSF) AWLR prototype. (a) Bandstop state. (b) All-pass state.

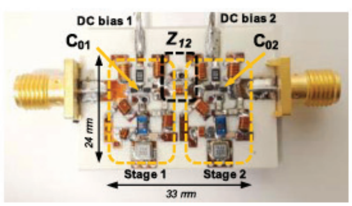

Fig. 6. Manufactured two-stage prototype. The SMD stages are identical to the ones in Fig. 4. Z_{12} was implemented with its low-pass equivalent: one inductor (0806SQ8N9) and two capacitors (251R14S3R3BV4T).

$<$ 0.38 dB and 2) a bandstop mode with a center frequency of 917.5 MHz, an FBW of 0.29% (2.4 k_t^2), and a stopband isolation (IS) of 21.2 dB. The IL is mostly attributed to the loss of the thru-line. It is higher in the bandstop state due to the phase of the line being altered by only tuning its capacitance which results in reflection loss. A comparison with the EM-simulated responses (AWRs modeled by the BVD model in Fig. 1) is also provided which as shown is in a good agreement. The ripples in the measurements are due to the multimode nature of the SAW resonator as also observed in the filters in [2]–[7]. The manufactured two-stage prototype and its RF-measured bandstop and all-pass modes are shown in Figs. 6 and 7, respectively. Its RF performance metrics can be summarized as follows. All-pass mode: IL $<$ 0.67 dB. Bandstop mode: a center frequency of 916.9 MHz and an FBW of 0.47% (3.8 k_t^2). A comparison with its corresponding EM-simulated response is also provided. As shown, the selectivity of the two-stage prototype is higher than in the one stage, which validates the scalability of this concept to multistage realizations. Furthermore, the obtained FBWs are wider than k_t^2, demonstrating its capabilities for enhanced FBW stopbands. Lastly, Fig. 8 illustrates the potential to tune the IS of the two-stage prototype by altering θ_1, θ_2. This is achieved by varying the varactors' biasing which results in a tunable IS between 20 and 43 dB. A comparison of the proposed filter concept with alternative reconfigurable transfer-function AWRs and filters is provided in Table II. As shown, this is the only AWR filter that allows all-pass-to-bandstop reconfigurability with continuously tunable IS and enhanced FBW.

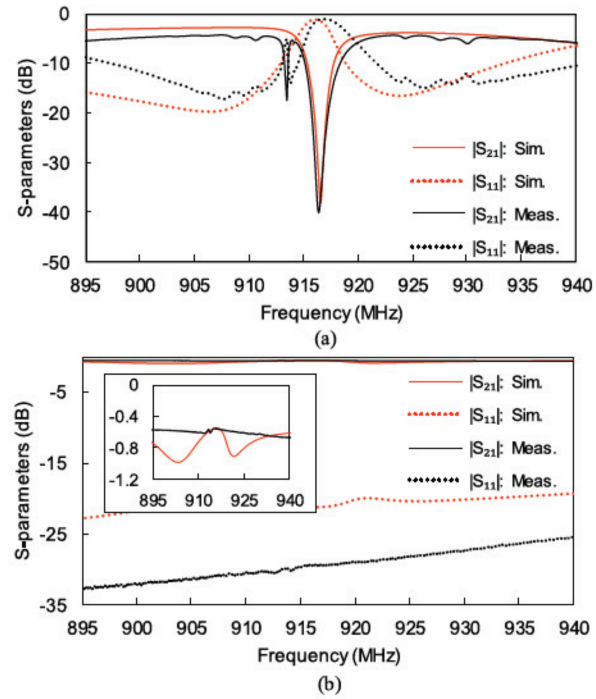

Fig. 7. RF-measured and EM-simulated S-parameters of the two-stage all-pass-to-BSF AWLR prototype. (a) BSF state. (b) All-pass state.

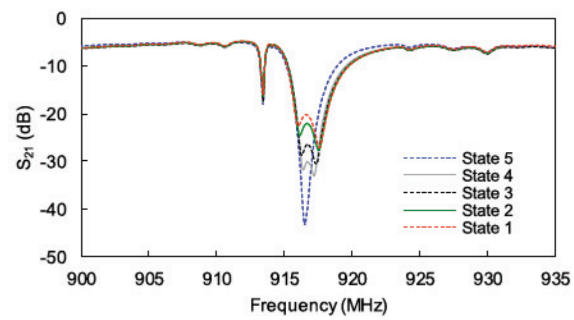

Fig. 8. Reconfigurable measured states of the two-stage prototype. They were obtained by electronically reconfiguring C_{01}, C_{02}.

TABLE II

TRANSFER-FUNCTION-RECONFIGURABLE AWRS AND AWR FILTERS

Ref.	Technology	Rec. modes	f_{cen} (MHz)	FBW (xk_t^2)
T.W	SAW & LE filter	AP/BS/Tun. IS	917.5	2.7-3.3
[7]	FBAR filter	BP/AS	2000	0.5
[8]	AlGaN Resonator	BP/AS	246	N/A
[12]	AlN Resonator	BP/AS	640	N/A

LE: lumped-element, AP: all-pass, AS: all-stop, BS: bandstop, BP: bandpass

IV. CONCLUSION

This letter discussed the design and practical development of reconfigurable AWLR-based all-pass-to-bandstop filters. They are based on in-series cascaded tunable all-pass-to-bandstop stages that facilitate the realization of: 1) a low-IL all-pass mode of operation and 2) a bandstop mode with enhanced FBW stopband and reconfigurable isolation levels. The operating principles of the all-pass-to-bandstop concept were verified by a single-stage and a two-stage reconfigurable prototypes.

REFERENCES

[1] R. Ruby, "A snapshot in time: The future in filters for cell phones," *IEEE Microw. Mag.*, vol. 16, no. 7, pp. 46–59, Aug. 2015.

[2] C. C. W. Ruppel, "Acoustic wave filter technology—A review," *IEEE Trans. Ultrason., Ferroelectr., Freq. Control*, vol. 64, no. 9, pp. 1390–1400, Sep. 2017.

[3] Y. Yang, R. Lu, L. Gao, and S. Gong, "4.5 GHz lithium niobate MEMS filters with 10% fractional bandwidth for 5G front-ends," *J. Microelectromech. Syst.*, vol. 28, no. 4, pp. 575–577, Aug. 2019.

[4] S. Doberstein, "Switchable low-loss SAW filter banks with MEMS switches," in *Proc. IEEE Int. Ultrason. Symp.*, San Diego, CA, USA, Oct. 2010, pp. 1294–1297.

[5] H. Hirano *et al.*, "Bandwidth-tunable SAW filter based on wafer-level transfer-integration of $BaSrTiO_3$ film for wireless LAN system using TV white space," in *Proc. IEEE Int. Ultrason. Symp.*, Sep. 2014, pp. 803–806.

[6] M. Z. Koohi, S. Lee, and A. Mortazawi, "Compact intrinsically switchable FBAR filters utilizing ferroelectric BST," *IEEE Trans. Ultrason., Ferroelectr., Freq. Control*, vol. 65, no. 8, pp. 1468–1474, Aug. 2018.

[7] M. Z. Koohi, S. Nam, and A. Mortazawi, "Intrinsically switchable and bandwidth reconfigurable ferroelectric bulk acoustic wave filters," *IEEE Trans. Ultrason., Ferroelectr., Freq. Control*, vol. 67, no. 5, pp. 1025–1032, May 2020.

[8] L. C. Popa and D. Weinstein, "Switchable piezoelectric transduction in AlGaN/GaN MEMS resonators," in *Proc. Transducers Eurosensors XXVII, 17th Int. Conf. Solid-State Sens., Actuators Microsyst. (TRANSDUCERS EUROSENSORS XXVII)*, Barcelona, Spain, Jun. 2013, pp. 2461–2464.

[9] D. Psychogiou, R. Gómez-García, and D. Peroulis, "Single and multiband acoustic-wave-lumped-element-resonator (AWLR) bandpass filters with reconfigurable transfer function," *IEEE Trans. Microw. Theory Techn.*, vol. 64, no. 12, pp. 4394–4404, Dec. 2016.

[10] D. Psychogiou and D. J. Simpson, "Multi-band acoustic-wave-lumped-element resonator-based bandstop filters with continuously tunable stopband bandwidths," in *IEEE MTT-S Int. Microw. Symp. Dig.*, Philadelphia, PA, USA, Jun. 2018, pp. 860–863.

[11] N. S. Luhrs, D. J. Simpson, and D. Psychogiou, "Multiband acoustic-wave-lumped-element resonator-based bandpass-to-bandstop filters," *IEEE Microw. Wireless Compon. Lett.*, vol. 29, no. 4, pp. 261–263, Apr. 2019.

[12] C. D. Nordquist *et al.*, "MEMS switching of contour-mode aluminum nitride resonators for switchable and reconfigurable radio frequency filters," *J. Micromech. Microeng.*, vol. 26, no. 10, Oct. 2016, Art. no. 104001.